CZECH TECHNICAL UNIVERSITY IN PRAGUE

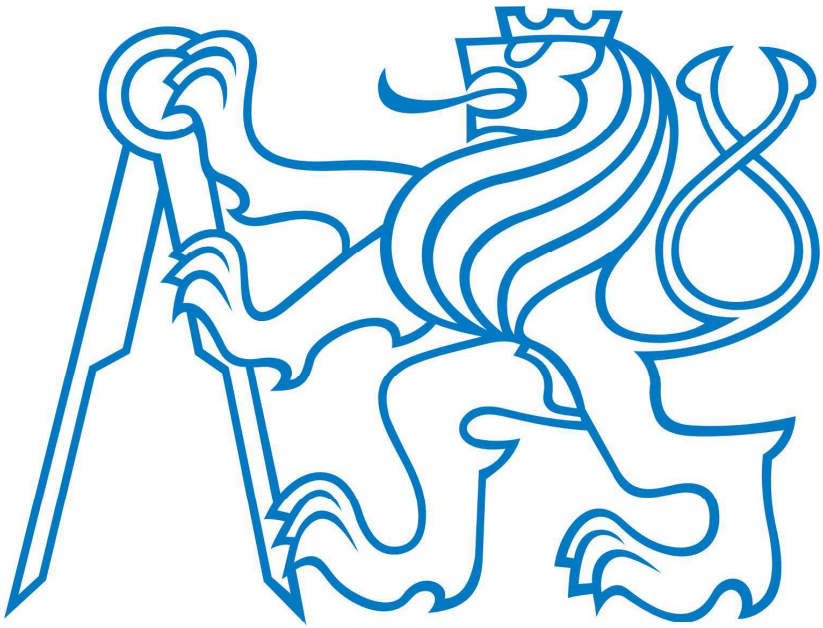

DOCTORAL THESIS STATEMENT

Czech Technical University in Prague

Faculty of Electrical Engineering

Department of Electromagnetic Field

Jiří Libich

DIVERSITY TECHNIQUES FOR FREE SPACE OPTICAL NETWORKS

Ph.D. Programme:

Electrical Engineering and Information Technology

Branch of study: Radioelectronics

Doctoral thesis statement for obtaining the academic title of "Doctor", abbreviated to "Ph.D."

Prague, August 2013

The doctoral thesis was produced in full-time manner Ph.D. study at the department of electromagnetic field of the Faculty of Electrical Engineering of the CTU in Prague

Candidate: Ing. Jiří Libich

Department of Electromagnetic Field
Faculty of Electrical Engineering of the CTU in Prague
Technická 2, 166 27 Prague 6

Supervisor: Doc. Ing. Stanislav Zvánovec Ph.D.

Department of Electromagnetic Field
Faculty of Electrical Engineering of the CTU in Prague
Technická 2, 166 27 Prague 6

Supervisor-Specialist: Doc. Ing. Karel Novotný

Department of Electromagnetic Field
Faculty of Electrical Engineering of the CTU in Prague
Technická 2, 166 27 Prague 6

Opponents:

The doctoral thesis statement was distributed on:

The defence of the doctoral thesis will be held on ..... at ..... a.m./p.m. before the Board for the Defence of the Doctoral Thesis in the branch of study Radioelectronics in the meeting room No. ..... of the Faculty of Electrical Engineering of the CTU in Prague.

Those interested may get acquainted with the doctoral thesis concerned at the Dean Office of the Faculty of Electrical Engineering of the CTU in Prague, at the Department for Science and Research, Technická 2, Praha 6.

Chairman of the Board for the Defence of the Doctoral Thesis
in the branch of study Radioelectronics
Faculty of Electrical Engineering of the CTU in Prague
Technická 2, 166 27 Prague 6

CURRENT SITUATION OF THE STUDIED PROBLEM

Free space optical technology has gone through long time development. Theoretical models of optical beam propagation in case of weather events such as rain, snow, fog as well as turbulence in the atmosphere have been developed [1, 2, 3, 4, 5, 6]. Also optoelectronics is growing rapidly and new parts are available for new designs. This chapter summarizes current available FSO technology, influences on propagation of the optical beam and propagation models.

Atmospheric Influence on Optical Beam Propagation

Propagating optical beam interacts with the atmosphere owing to its composition consisting of variety molecules and particles. The interaction causes extinction of the optical beam. Extinction is defined as a decrease of the optical beam intensity and it is caused by absorption and scattering. It can be subdivided into two size domains: molecular and aerosol extinction. The atmospheric extinction coefficient γ is defined as the sum of the atmospheric absorption α and scintillation β coefficient [1].

$$\gamma(\lambda, l) = \alpha(\lambda, l) + \beta(\lambda, l) \tag{1}$$

Fog Attenuation

Aerosols are small particles of size within the range of 0.002 to 100 μm, for example aerosols are fog, smoke, haze, maritime spindrift particles and see salt, soil and rock debris etc. Aerosol extinction depends on the size, composition and number of particles in the volume unit. The lifetime of the aerosols is dependent on the particle size. Assuming non-turbulence medium and only gravitational and drag forces, steady-state or terminal settling velocity can be determined.

The absorption coefficient $\beta_n(\lambda)$ is given by following equation [7]

$$\beta_n(\lambda) = 10^5 \int_0^\infty Q_d\left(\frac{2\pi r}{\lambda}, n'\right) \pi r^2 \frac{dN(r)}{dr} dr \tag{2}$$

where λ is the wavelength, $dN(r)/dr$ introduces the particle size distribution per unit volume, n' stands for the real part of the refractive index n of the aerosol, r (cm) denotes the radius of the particles and $Q_d(2\pi r/\lambda, n')$ means the scattering cross section for a given type of aerosol. The coefficient Q_d can be determined based on Mie theory. The theory assumes that particles are spherical and sufficiently distant from each other for far field mode calculation. The key parameter is size of the aerosol compared to wavelength is given by [1]

$$x = \frac{2\pi r}{\lambda} \tag{3}$$

The scattering cross section Q_d is dependent on the parameter x and reaches maximum value when the particle radius equals the wavelength of the incident light. There are severa models of aerosol scattering. The scattering coefficient is related to the meteorological visibility V by the following equation [3, 4, 8]

$$\beta_n(\lambda) = \frac{3.91}{V}\left(\frac{\lambda}{550nm}\right)^{-q} \tag{4}$$

where q denotes a coefficient dependent on the size distribution of the scattering particles. Modified model defined by Kim [3, 4] defines the parameter q as:

$$q = \begin{cases} 1.6 & V > 50km \\ 1.3 & 6km < V < 50km \\ 0.16V + 0.34 & 1km < V < 6km \\ V - 0.5 & 0.5km < V < 1km \\ 0 & V < 0.5km \end{cases} \tag{5}$$

Al Naboulsi model distinguishes advection and radiation fog. The scattering coefficient for advection fog is given by [9]

$$\beta_{ADV}(\lambda) = \frac{0.11478\lambda + 3.8367}{V} \tag{6}$$

Coefficients given by Al Naboulsi model for radiation fog are [9]

$$\beta_{RAD}(\lambda) = \frac{0.18126\lambda^2 + 0.13709\lambda + 3.7502}{V} \tag{7}$$

Fog and haze consist of small water droplets with size up to 100 μm and they have character of aerosols. If the temperature of the air falls below a dew point, the air is saturated and water vapor contained in the air condenses in fine water droplets. Attenuation of fog can be therefore determined on dependent meteorological visibility by Equation 4.

Many measurements under various weather conditions were carried out. Characterization of channel properties for rain is discussed in [10]. Comparison of rain, fog and haze with theoretical models is examined in [11]. Fog attenuation dependent on meteorological visibility is summarized in [8].

Comparison of attenuation with models based on visibility mentioned above is shown in Figure 1.

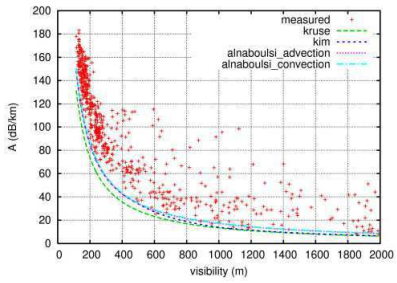

Figure 1: Comparison of measured attenuation with theoretical models [12].

Rain and Snow Attenuation

Rain consists of water droplets having various in the size, number and the space distribution. The shape of a raindrop is dependent on its size and it graduates from sphere to flatted ellipsoid. In infrared region, wavelength is much smaller than the diameter of the droplet. Total attenuation by rain is dependent on the quantity of raindrops in propagation path. The size distribution is commonly determined by Marshall-Palmer distribution [7]

$$N(r) = N_0 e^{-\gamma r} \tag{8}$$

where $N(r)$ stands for number of droplets per unit volume whose equivalent radius lies between r and $r + dr$. $N_0 = 16 \times 10^3$ m^{-3}mm^{-1} and $\gamma = 8.2R^{0.21}$ where R is the rain intensity in mm/h. The parameters depend on type of rain and they are experimentally determined. Attenuation A_{prec} in db/km caused by rain can be expressed as a function of the rain intensity R in mm/h as [13]

$$A_{prec} = kR^{\alpha} \tag{9}$$

where parameters $k = 1.076$ and $\alpha = 0.67$ (for France) depend on rain characteristics [2], ([14] introduces $k = 4.9$ and $\alpha = 0.63$ meausred in Tokio, Japan).

Snow consists of snowflakes or ice crystals. Size of a snowflake can reach up to 15 mm and it has no defined form. It is defined as water volume after melting corresponding to the sphere water droplet. Attenuation is strongly dependent on snow density and humidity. Dry snow attenuation can reach up to 50 dB/km whereas attenuation caused by wet snow is approximately in range of 4 to 8 dB/km.

Specific attenuation γ_{snow} caused by snow determines following relation [7]

$$\gamma_{snow} = aS^{b} \tag{10}$$

Parameters a and b for wet and dry snow are introduced in Table 1.

Table 1: : Parameters a and b for wet and dry snow.

	a	b
Wet snow	0.000102 $\lambda_n m$ + 3.79	0.72
Dry snow	0.0000542 $\lambda_n m$ + 5.50	1.38

Figure 2a shows specific attenuation due to rain and Figure 2b depicts specific attenuation of wet and dry snow in dependence on precipitations calculated using Equation 9 and 10.

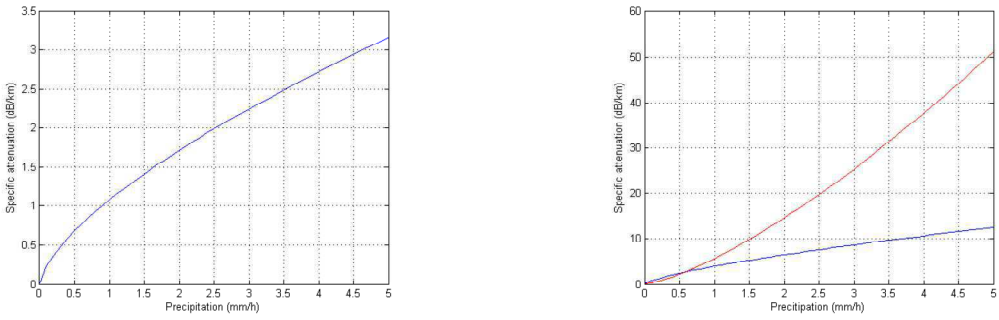

(a) (b)

Figure 2: Specific attenuation due to: a) rain; b) wet (blue line) and dry (red line) snow.

Scintillation

Turbulence within propagation media result in variance of the refractive index and its inhomogeneity within the space and time which causes scintillation and beam wandering. The received optical power is fluctuating at the frequency range from 0.01 to 200 Hz [15]. The wave front is

deformed and the optical beam wanders and it is broadened. The frequency and amplitude of scintillation depend on cells diameter to beam diameter ratio. Random speed of fluctuation of a fluid results in turbulence. In the atmosphere, there are two different type of motion, laminar and turbulent. In contrary to laminar flow, turbulent flow is the cause of constant dynamic mixing of media and creates smaller flow areas called eddies which occupy areas from tens of centimeters to units of kilometers. Type of flow can be determined by Reynolds number which gives a measure of the ratio of inertial forces to viscous [15]. Transition from laminar to turbulent flow is depicted in Figure 3a.

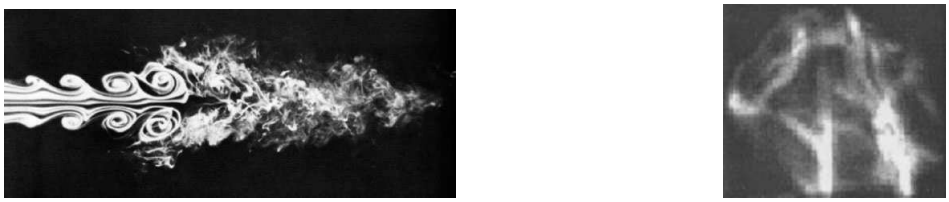

(a) (b)

Figure 3: a) Transition from the laminar to the turbulence flow; b) laser beam footprint after passing through turbulence media [1].

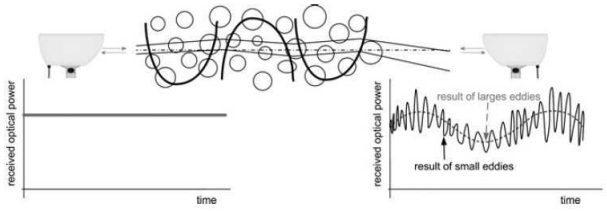

Figure 4: Demonstration of the turbulent atmosphere influence on a free-space optical link [6]

The variance σ_χ^2 of optical intensity is represented by Rytov variance expressed by the next equation [5]

$$\sigma_\chi^2 = AC_n^2 \left(\sqrt[6]{\left(\frac{2\pi}{\lambda}\right)^7 L^{11}} \right) \tag{11}$$

where constant A is 1.23 in case of plane wave propagation and 0.5 for spherical wave, λ introduces the wavelength and L is the length of the optical beam path, C_n^2 stands for the refractive index structure parameter and it can be derived from temperature structure function $D_T(R)$ using [15]

$$D_T(R) = \left\langle (T_1 - T_2)^2 \right\rangle = \begin{cases} C_T^2 R^{2/3}, l_0 < R < L_0 \\ C_T^2 l_0^{-4/3} R^2, R < l_0 \end{cases} \tag{12}$$

Turbulence Models

Power fluctuation of the received optical signal is usually described by statistical models. The most widely used statistical models include lognormal distribution, K-distribution and gamma-gamma distribution. Weak turbulences have lognormal distribution while K-distribution is used for strong turbulences [16].

Log-normal distribution
Log-normal distribution is defined as

$$f(I) = \frac{1}{\sqrt{2\pi}\sigma_l I} \exp\left\{ \frac{\left(\ln {}^{I}/_{I_0} + {}^{\sigma_l^2}/_{2}\right)^2}{2\sigma_l^2} \right\}, I > 0 \tag{13}$$

where σ_l^2 is the scintillation index, I and I_0 denotes irradiance (intensity of the optical wave) and its mean value in cases without turbulence, respectively. $K_{\alpha-1}(..)$ stands for a modified Bessel function of the second kind, $\Gamma(..)$ is the gamma function and α introduces the effective number of discrete scatters.

Gamma-Gamma distribution
Under the assumption that small-scale irradiance fluctuations are modulated by large-scale irradiance fluctuations of the propagating wave, gamma–gamma distribution can be utilized in a free-space optical channel.

$$f(I) = \frac{2(\alpha\beta)^{\frac{(\alpha+\beta)}{2}}}{\Gamma(\alpha)\Gamma(\beta)} I^{\frac{\alpha+\beta}{2}-1} K_{\alpha-\beta}\left(2\sqrt{\alpha\beta I}\right), I > 0 \tag{14}$$

where α and β are effective numbers of small- and large-scale eddies [17].

The gamma-gamma distribution is normalized, i.e. $\langle I \rangle = 1$. Second moment is then $\langle I \rangle = (1 + 1/\alpha)(1 + 1/\beta)$. Scintillation index can be expressed by parameters α and β

$$\sigma_I^2 = \alpha^{-1} + \beta^{-1} + (\alpha\beta)^{-1} \tag{15}$$

Assuming plane wave propagation, α and β can be expressed as [5]

$$\alpha = \frac{1}{\sigma_x^2} = \left[\exp\left(\frac{0.49\sigma_\chi^2}{\left(1 + 1.11\sigma_\chi^{12/5}\right)^{7/6}} \right) - 1 \right]^{-1} \tag{16}$$

$$\beta = \frac{1}{\sigma_y^2} = \left[\exp\left(\frac{0.51\sigma_0^2}{\left(1 + 0.69\sigma_\chi^{12/5}\right)^{7/6}} \right) - 1 \right]^{-1} \tag{17}$$

Measurement of scintillations and BER performance were investigated and published in [18, 19, 20, 21].

Diversity Techniques

Unfortunately, atmospheric and weather effects such as rain, fog or turbulence (refer to Chapter) negatively influence laser beam propagation through the atmosphere. It results in loss of energy of the optical beam in direction of propagation and optical signal degradation, for instance wave-front distortion. Several mitigation techniques were proposed including adaptive optics, beam tracking or, as this chapter discuss, different types of diversity techniques [1]. Bit error rate (BER) also can be increasing by using of convenient codes or more robust modulation techniques in the upper layers of the OSI model. Three diversity techniques, well known from

RF links, are usually used in FSO. It includes wavelength, spatial and route diversity technique which are described below.

Route Diversity

FSO systems also can be involved into complex networks for interconnecting buildings of campuses, several buildings of companies or a hospital complex in various network topologies containing distinct FSO and RF systems. Availability of the whole network depends on each component and on arrangement of links. As it is known from other networks, physical topology of the network include ring topology, star topology and mesh topology.

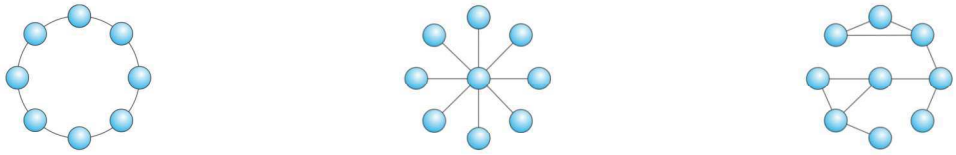

(a) Ring topology (b) Star topology (c) Mesh topology

Figure 5: Possible configuration of a FSO network

Ring topology As it is shown in Figure 5a, this network architecture is based on connection of all links into closed ring. In case of failure a link, the other links in the network are used to provide the connection. Thus the availability can be increased.

Star topology
In star networks, all links are connected to the central point of the network (Figure 5a). Because a common FSO link is designed as point to point link, central point have to consist of several FSO links, each for every link. Therefore the current research is focused on development of multipoint central unit [1]. It can be reached by wide beam angle light source or multiple transmitter optics. But this concept has a big disadvantage. In case of central unit failure, whole network is then unavailable.

Mesh topology
More complex network architecture combining both above discussed topologies, known as mesh topology, provide the best solution to ensure high value of availability. Owing to multiple existing connections, during a link failure, another possible connection can be used. This situation is depicted in Figure 6a.Figure 6b depicts the received optical power with marked thresholds as criterion to network reconfigure with hysteresis. Once the received optical power fall under the threshold T_0, the network is reconfigured and another available link is used (FSO or RF) to maintain connection. When the received optical power reaches threshold T_1, the original link is used again. This method requires continuous monitoring of the received optical power, which is not available for each FSO terminal. In this case it can be used simple connection test (using ping tool for instance) and the network is then reconfigured at connection outage.

(a) (b)

Figure 6: a) Simple FSO network, b) the threshold criterion [22].

According to [23], the reconfiguration probability derived from the Gamma-Gamma distribution model (defined above) may me expressed as

$$\pi_n\left(S_2\right) = \frac{2(\alpha\beta)^{(\alpha+\beta)/2}}{\Gamma\left(\alpha\right)\Gamma\left(\beta\right)} \int_0^{\sqrt{\frac{\gamma_L}{\bar{\gamma}}}} h^{\frac{\alpha+\beta}{2}-1} K_{\alpha-\beta}\left(2\sqrt{\alpha\beta h}\right) dh \tag{18}$$

where Γ_L accords to lower SNR treshold level, when the link is reconfigurated to another one (Γ_H denotes the higher SNR level, when the original link is used) and $\bar{\gamma}$ stands for average SNR.

Please note that S_0, S_1 and S_2 denotes normal operational state, hysteresis and reconfigurated state, respectively.

Using Meijer's G-function to solve the integral, the equation is derived as

$$\pi_n\left(S_2\right) = 1 - \frac{(\alpha\beta)}{\Gamma\left(\alpha\right)\Gamma\left(\beta\right)}\left(\alpha\beta\sqrt{\frac{\gamma_L}{\bar{\gamma}}}\right)^{\frac{\alpha-\beta}{2}} G_{1,3}^{3,0}\left[\alpha\beta\sqrt{\frac{\gamma_L}{\bar{\gamma}}}\,\middle|\, \begin{matrix} -\frac{\alpha+\beta}{2} \\ 1-\frac{\alpha+\beta}{2}, \frac{\alpha-\beta}{2}, \frac{\beta-\alpha}{2} \end{matrix}\right] \tag{19}$$

If it is assumed a mesh network with N nodes, the reconfiguration probability matrix between nodes n and m is defined in [23].

Probability of node failure with K_n active FSO links can be expressed by

$$\tilde{P}_r^{(n)} = \prod_{i=1}^{K_n} P_r^{n,i} \tag{20}$$

AIMS OF THE DOCTORAL THESIS

The objective of the dissertation thesis is to find propagation model of FSO mesh networks utilizing route diversity based on long-term measurement of atmospheric conditions and corresponding characteristics of optical beam propagation using outdoor and indoor experimental FSO links. This model is related to the location of the urban area. Although propagation of the optical beam within the atmosphere is very well described, the use of FSO mesh network to mitigate of harmful effects is not well described. First of all, new measurement network consist of three FSO links was proposed and realized at the Czech Technical University (CTU) in Prague in cooperation with Orlik and Bubenec Dormitories. Two new FSO links was deployed on the roof of the university building and Orlik dormitory and the third existing FSO link between CTU and Bubenec dormitory was included to the network. Two meteorological stations was extended by a visibility sensor and temperature sensor set measuring temperature gradients within the atmosphere, which was developed as part of this work. Software for data capturing and storing was developed in order to long-time measurement of atmospheric characteristics and received optical power measurement. To extend outdoor measurement, laboratory experiments was carried out in order to investigate individual effects separately under defined conditions.

The dissertation thesis was focused on following objectives:

- Analysis of route diversity in FSO newtworks
- To find a diversity model based on experimental measurements
- Specify diversity model by laboratory measurements

WORKING METHODS

Outdoor Measurement

Experimental measurement campaign was set up at the university campus of the Czech Technical University in Prague (CTU) in order to derive a novel model of beam reception statistics in FSO networks which use route diversity to mitigate influence of the atmosphere. Three FSO links are placed on the roof of the university building together with meteorological sensors and connects campus with dormitories and mechanical engineering faculty's building part. The measurement set-up is depicted in Figure 7a. All FSO links work at the wavelength of 850 nm and allow to capture received optical power every second. Figure 7b depicts node 2 with LightPointe Strata MRV TeleScope

(a) (b)

Figure 7: a) deployment of FSO network at the CTU in Prague; b) detail of node 2.

Link A is Wavebridge 500 by Plaintree corporation. It is also planned to use the same FSO link to directly interconnect Orlik and Bubenec dormitory in order to finish a simple mesh network. This FSO unit uses an LED as optical source with output optical power of 20 dBm and 17 mrad beam divergence. The received signal strength indication (RSSI) is used to the received optical power measurement.

Link B is Lightpointe Strata G FSO terminal. It is a four beam FSO link (4×4 MIMO). This FSO link can carry data up to rate 1.25 Gbps. As optical sources are used VCSEL laser diodes with output power of 7.8 dBm each (13.8 dBm total power) and 2 mrad divergence. The receivers are consist of Si APD photodetectors. The receiver sensitivity is -30 dBm for BER 10^{-10}.

Link B is equipped with radio frequency backup communication system working at license free frequency of 5 GHz. Both links are monitored by SNMP protocol (Strata terminal is monitored using LightPointe FMG unit connected by multimode optical fiber). Beside the received optical power, the FSO link offer other information such as connection time and total working time, which allow us to determine the availability and other indicators. These links are use in real traffic. Scheme of this node is depicted in the Figure 8. Together with another WaveBridge form connection to Orlik dormitory.

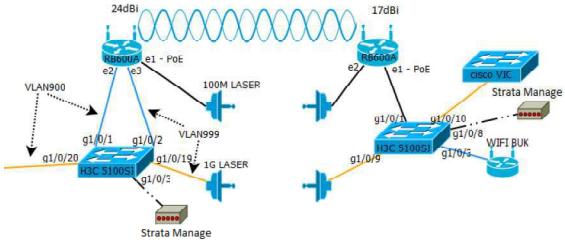

Figure 8: Schematic diagram of link B, left part is placed at the dormitory and right part at CTU.

Reconfiguration of the network owing fading is ensured by Mikrotik router on the side of Orlik dormitory. It send ping requests every second through Strata link to the gateway and if it does not receive the answer for 10 seconds, it try to connect through the second FSO. If even in this case the answer is not received, the network is reconfigured to use RF backup link. When the Strata link is available again, the network configuration change back to default setting.

Link C is MRV Telescope 700. The transmitter is equipped with a VCSEL laser diode with 7 dBm output power and 3.5 mrad divergence. Si phododiode has sensitivity of -32 dBm. Maximum data-rate is 155 Mbps. Like the link A, RSSI is used to measure the received optical power. Because documentation of neither link A nor link C do not provide relationship between RSSI and the received optical power, both links was calibrated and the relative optical power was interpolated against different values of RSSI. To determine of relative attenuation during calibration, attenuation foil was used with known attenuation measured in laboratory.

Indoor Measurement

Modular optical chamber can be 1 to 5 m long (in 1 m steps) and allows to measure up to 4 independent (or partly independent) channels. Base plates are locked together and contain grooves for side plates. According to Figure 9, the chamber can be divided lengthwise or transversely into several independent or partially independent channels.

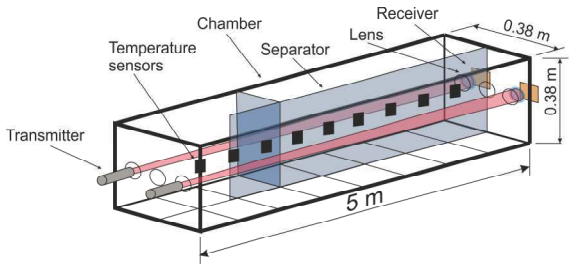

Figure 9: Example of experiment setup with basic components

Bit error rate tester (BERT) is being developed on FPGA evaluation board with Spartan 3E FPGA chip. It consist of a pseudo-random binary sequence (PRBS) generator and a receiver, which compares transmitted and received data and detects errors. The output LVDS (low level differential signaling) signal leads from FPGA board to SFP module working at the wavelength of 850 nm, which is used as optical source. It can also modulates laser module Beta TX, which is used and described in experiment mentioned below. Data rate is adjustable from 1 Mbps to 50 Mbps.

Rhode&Schwarz SMIQ 03B generator, which allow to use of several types of modulations, was used to modulate laser Beta TX module working at the wavelength of 850 nm. Optical beam

was influenced by 2 kW heaters and focused on detector Thorlabs PDA10CF-EC using a lens with focal length of 50 mm. Electrical signal was demodulated by spectrum analyzer Agilent E4440A.

RESULTS

Outdoor Measurement

Influence of Buildings

Optical beam propagation within street corridors is also affected by surrounding building. If an optical link is installed on the roof, temperature gradients caused by for example cooling air conditioning unit create additional turbulence source. In a similar way optical beam can be influenced above roofs with chimneys, which can produce smog.

Compared to log-normal measurement statistics presented for several maritime links in [24], the normalised scintillation index (by a mean value of 0.013) was not as strictly followed by a fitted log-normal cumulative function in our measurement (see the cumulative probability of normalised scintillation index from September 2010 depicted in Figure 10a. For higher scintillation indices (cumulative probabilities higher than 0.94) the gamma–gamma statistical approach dominates. The fit error calculated according to [24] as the difference between measured data and the particular statistical model is shown in Figure 10b In the case of the log-normal model, the overall fitting quality measure – RMS error – reached a value of 0.0239. This is quite a huge difference from the theoretical assumption – compared to [24], where RMS errors were almost ten times smaller in case of maritime optical links having lengths 6, 9.4, 17.7 and 23.6 km. The worst fit was observed with the gamma-gamma statistical model, where an RMS error of 0.0409 was enumerated.

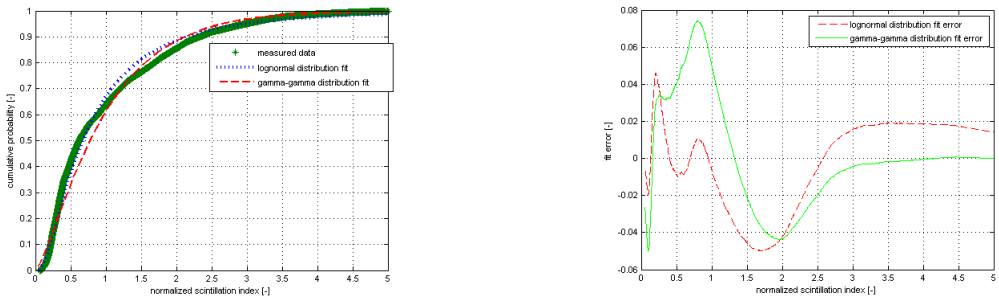

(a) (b)

Figure 10: Comparison of measured and theoretically derived statistics. a) cumulative probability of normalized scintillation index from September 2010; b) fit error between measured data and the calculated model.

Based on statistics derived from sensor line measurements, the thermal influence of buildings was analyzed. Significant thermal variations were observed along the measured path. At the beginning of the measurement campaign, undesirable heating of sensors by sunshine was distinguished. Therefore sensors was improved by an upper alumina shield with special holes enabling even top-down air circulation and new measurement will be proceeded.

To validate the influences of the turbulent zones, the refractive index structure parameter was determined from the thermal sensor line measured data using the empirical equation

$$C_n^2 = \left(79 \times 10^{-6} \frac{P}{T^2}\right) \frac{(T_1 - T_2)^2}{R^{C_{par}}} \tag{21}$$

where T_1 and T_2 stand for temperatures measured by two adjacent thermal sensors separated by a distance R, T represents mean temperature from all sensors and P introduces atmospheric pressure. Parameter C_{par} represents the thermal influence expressed by the so-called temperature structure function [25]. It characterizes the dissipation range (inertial range) from largest eddies expressed by diameter L_0 (up to outer scale of turbulence) towards the smallest ones with a diameter of l_0. $C_{par} = 2$ was determined for smaller sensor separations $R < l_0$ [5]. It has to be mentioned that in the above- mentioned cases, either the vertical profile of turbulence were measured by balloon thermal radiosondes or horizontal measurements were performed in an open area. Contrary to the above-mentioned open-field measurements, in our case, when the link passed a built up area, C_{par} tended to reach a value of 2 even in the dissipation range (more specifically $C_{par} = 1.96$ was optimized from Kolmogorov statistics of measured data). Therefore in the next analyses performed C_{par} was equal to 2.

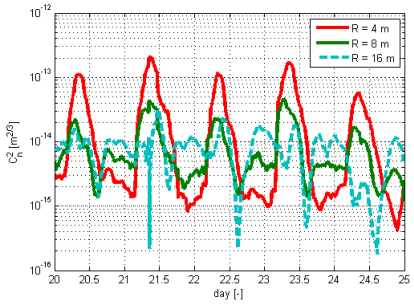

Figure 11: Refractive index structure parameter dependence for different distances from a building determined from thermal sensors line measurement in September 2010.

From the measured data, it was seen that turbulence emerges approximately in the first 1 to 2 meters surrounding buildings (derived from a two-month measuring period). A high influence on the fluctuation of the received optical signals can be observed from turbulence arising up to 8 m from the building. This is true especially during colder days, when the thermal heating of buildings radically changes the scintillation effects on a FSO link deployed in urban areas compared to links crossing free, non-built-up areas. Figure 12 depicts the relationship between the turbulence and the FSO received signal expressed by a mean correlation coefficient from a two-month observation period calculated by (21).

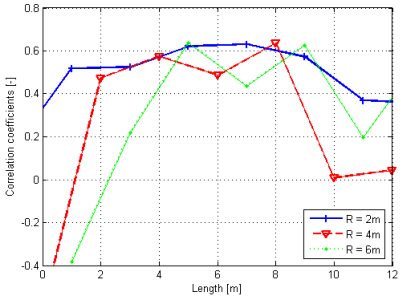

Figure 12: Dependence of the mean correlation coefficient between the refractive index structure parameter derived from FSO data and from thermal sensors based on sensor distance.

Hybrid FSO/RF Link

Propagation of optical beam is unfortunately affected by weather condition. During foggy days, attenuation of optical beam reaches up to hundreds of decibels per kilometer. It limits the use of the FSO technology during adverse weather conditions. In order to ensure high availability of a FSO link, it can be equipped with a backup radio link. One year measurement during 2012 and 2013 was carried out and data was analyzed to validate theoretical assumptions related to location of Prague. Data measured on the FSO link together with the backup radio link (described in Chapter) working at the wavelength of 850 nm and frequency of 5 Ghz, respectively, was collected from 23th May 2012 to 19th August 2013. Sample of measured data during several fog events from 19th to 22th October 2012 is depicted in Figure 13. The FSO link experienced high value of attenuation caused by fog event at night from 19th to 20th, which caused outage of the FSO link for three hours whereas the RF link worked normally.

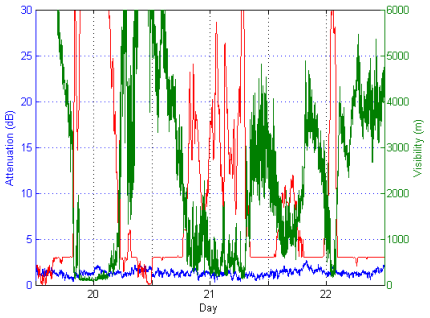

Figure 13: Comparison of measured attenuation the FSO (red line) and RF (blue line) link during fog event.

Availability was calculated from connection status (1 - connected, 0 - disconnected). Because the measurement was interrupted several times owing to technical problems, the table also indicates time percentage of the measurement. Overall availability of the FSO link was 99.7130 % (1 day and 8.4 hours a year) and RF link had availability of 99.9376 %. By combination of the FSO and RF link was reached availability of 100 %. Please note, that this value was determined from link status measured in one second interval and is dependent on given BER threshold. Moreover, data transmission through the RF link is slower than the FSO link. This disadvantage can be partially removed using RF links working at higher frequencies. Nevertheless, the microwave waves above 10 GHz are mainly attenuated by rain which must be taken into account when calculating a budget of the link.

Route Diversity in Mesh Networks

Probability density function (PDF) of measured data is depicted in Figure 14. Density functions was fitted using log-normal distribution with parameter μ and σ equal 0.1085, 0.3643; 0.0922, 0.4316; 0.6777, 0.8525 for link A, B and C, respectively.

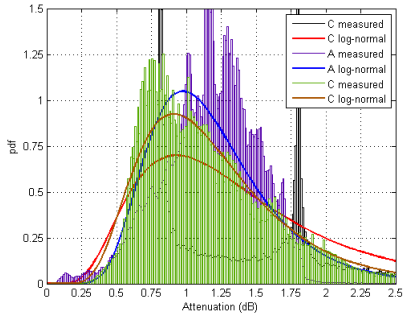

Figure 14: PDF of attenuation of FSO links A, B, C in June 2012 fitted by log-normal distribution.

Figure 15 shows survivor function of random data. It depicts characteristics of all FSO links and its minimum value. Diversity gain given by difference between individual characteristics and characteristic of minimum value is introduced in Table 2 for different time percentage.

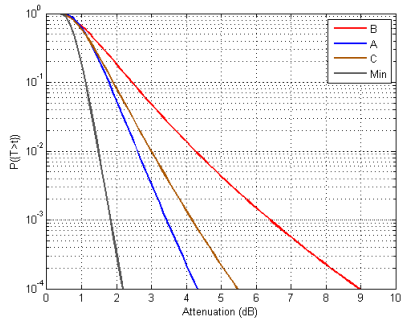

Figure 15: Survivor function of individual FSO link and minimal loss.

Table 2: Diversity gain of three FSO links.

Time (%)	***Diversity Gain (dB) of Link***		
	A	B	C
90.00	0.65	0.78	1.37
99.00	1.13	1.50	2.75
99.90	1.60	2.35	4.54
99.99	2.12	3.25	6.75

Figure 16a shows cumulative distribution function (CDF) of outages duration of the link B in case of link margin 10 dB. In 90% the outage long less than 40 seconds. Figure 16b illustrates PDFs of joint FSO links for particular fade margins. The outage statistic can be best approximated by a generalized extreme value distribution (GEV). GEV distribution is defined by following equation

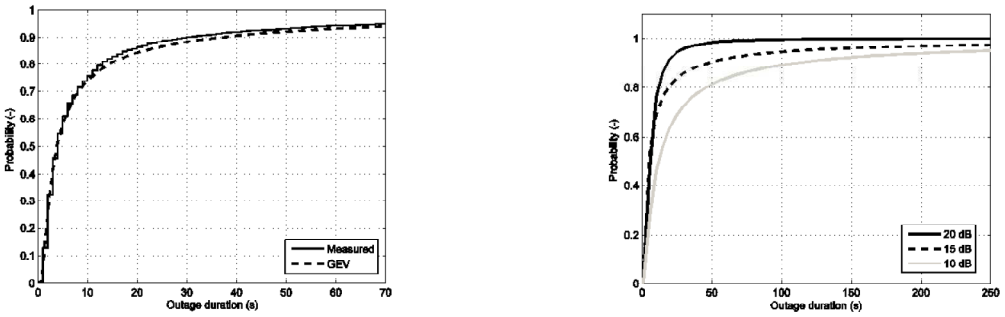

(a) (b)

Figure 16: Cumulative distribution function of outage duration of a) FSO link B; b) FSO links A and B in dependence on fade margin

Table 3: Parameters of GEV distribution fitted to outage duration.

Parameter	***Link B*** $T_0 = 20\ dB$	***Link A + B*** $T_0 = 20\ dB$	***Link A + B*** $T_0 = 15\ dB$	***Link A + B*** $T_0 = 10\ dB$
Location	0.85472	1.18469	1.17519	0.55828
Scale	2.78422	9.21363	3.76696	3.00408
Shape	2.93093	7.61219	3.60944	4.61317

Figure 17 shows probability density function of the refractive index structure parameter. It can be clearly seen, that strength turbulence is within weak regime. It implies that log-normal distribution is suitable for fitting of irradiance at the receiver.

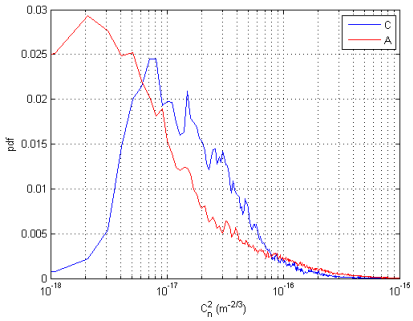

Figure 17: PDF of measured C_n^2.

Transverse coherence length of both channels is depicted in Figure 18a. Low values of the refractive index structure parameter result in high value of the coherence distance, which is important to determine proper diameter of receiver lens and separation between individual channels when using spatial diversity.

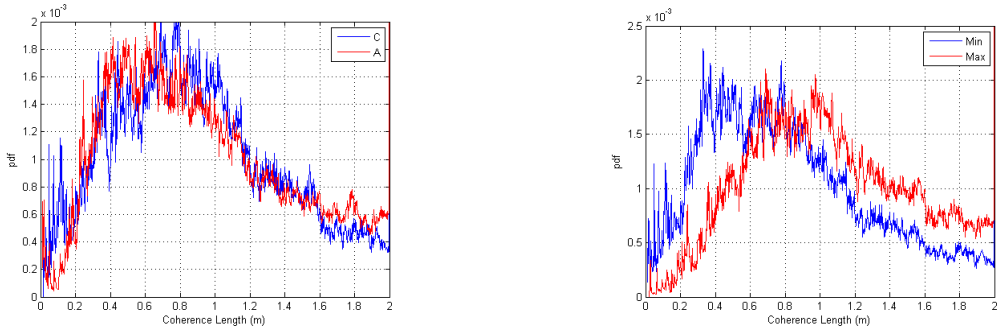

(a) (b)

Figure 18: a) PDF of coherence length of link A, B; b) PDF of minimal and maximal values of coherence length of link A, B.

Table 4 gives BER improvement of BPSK modulated signal using SelC method for $\mathcal{N} = 1, 2, 3$ at $\sigma_l^2 = 0.2$. In weak turbulence regime, contribution of SelC diversity is negligible compared to strong turbulence.

Table 4: BER improvement for $\mathcal{N} = 2, 3$ compared to one link at $\sigma_l^2 = 0.2$.

SNR (dB)	$\mathcal{N}$		
	1	2	3
20	4.72×10^{-4}	2.28×10^{-4}	2.01×10^{-4}
25	1.05×10^{-5}	1.37×10^{-6}	6.28×10^{-7}

Indoor Measurement

Turbulence Influence on Optical Beam Modulated by BPSK and 16QAM Modulation Techniques

Because this study have not been published yet, only several characteristic curves of measured data are presented. Optical beam propagating through the optical chamber was influenced by turbulence generated by heaters with a fan. This heaters was gradually placed at the transmitter and at the receiver side. In the first case, propagation of a BPSK signal was investigated. The profile of the refraction index structure parameter derived from temperature sensors is depicted in Figure 19. The strength of turbulence gradually increased in time, hence the analysis for several values of the refraction index structure parameter was carried out. The red line correspond to generating of turbulence at the transmitter which is placed in the zero distance and the blue line is for turbulence generated at the receiver.

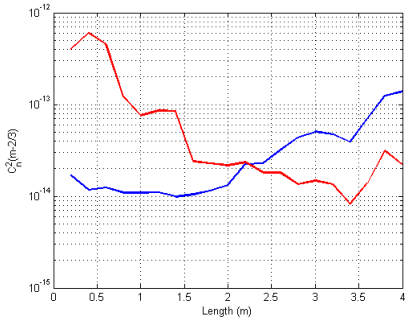

Figure 19: Sample of C_n^2 distribution during the experiment.

Next figure displays eye diagrams of 16QAM modulated signal again for two strengths of turbulence. As it was expected, strong turbulence at the transmitter cause high distortion of the received signal. In comparison to BPSK modulation, 16QAM modulation is highly affected by generated turbulence clearly seen when the signal is influenced at the transmitter with strong turbulence.

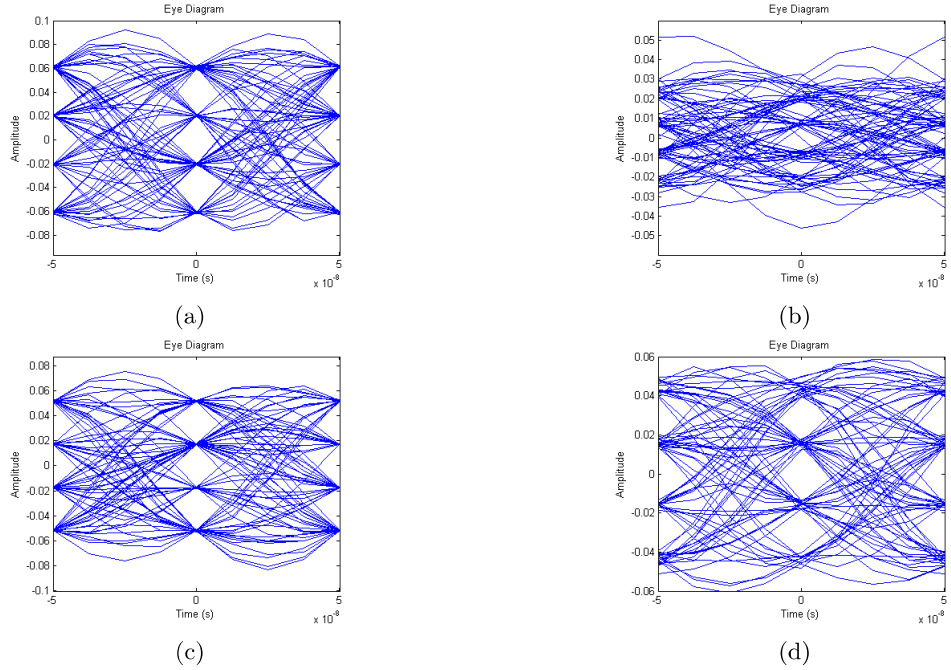

Figure 20: Eye diagram of 16QAM modulated optical beam for different strength of turbulence a) b) at the transmitter; c) d) at the receiver.

Route Diversity Analyses for Free-Space Optical Wireless Links Within Turbulent Scenarios

Separated Channels

A number of techniques have been proposed in the literature to deal with the turbulence including the aperture averaging, the spatial diversity, and the cooperative diversity, as mentioned in the introduction section. As a first analysis, in this paper a pilot testing measurement was performed with multiple transmitters. Within the measured scenario the laser beam at 830 nm was split into two with each beam propagating through two 1 m long non-turbulent and turbulent channels and then through a 1 m long common channel, see Figure 21a. The reduced

scintillation effect observed is mainly due to a small part of the propagation path being affected by different turbulence conditions. The diversity scheme was evaluated via a diversity gain, which is defined as the difference between attenuation of a single link and the minimum attenuation of joint diversity links. The diversity gain of the co propagating beams received by the receivers separated by 0.08 m did not exceed 0.4 dB even in case of the turbulence condition with $C_n^2 > 10^{-11}$ m$^{-2/3}$. Therefore for the small scale turbulence phenomena it would be more beneficial to employ the aperture averaging scheme. To validate statistical results, the channel separation was increased and measurements were carried out for two separate channels isolated by a divider and foils. The measurement set-up within the turbulence chamber is shown in Figure 21b. Channel 2 was influenced by a constant distortion or the impairment due to the intensity variation of the received signal, i.e. with Rytov variance being kept below 0.09. This small intensity variation is not considered to be due to the turbulence and is more to do with the material used to isolate both channels. In this case the foil is a transparent film sheet made of polyethylene terephthalate or polyester. The physical vibration of the foil is not significant to the human eye but does modify the intensity of the received signal, thus implying a small measured value of Rytov variance in the channel under study, however this small deviation and variance is not associated with the temperature effects. On the other hand, the turbulence in the channel 1 was gradually changed from low to moderate conditions.

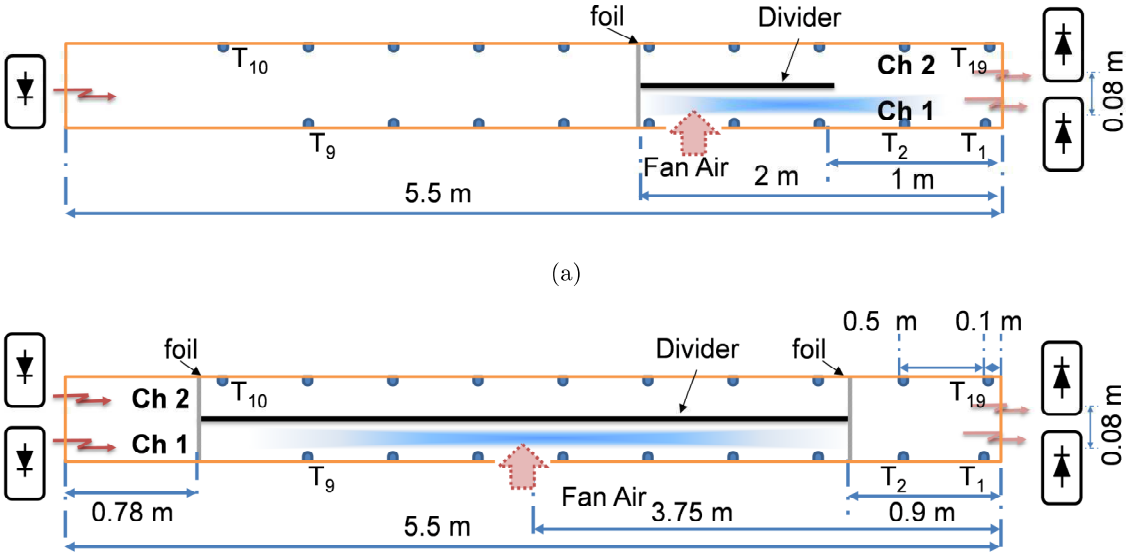

Figure 21: Deployment for measurement of two separated channels. a) unique laser source SIMO; b) dual laser source for isolated channels configuration.

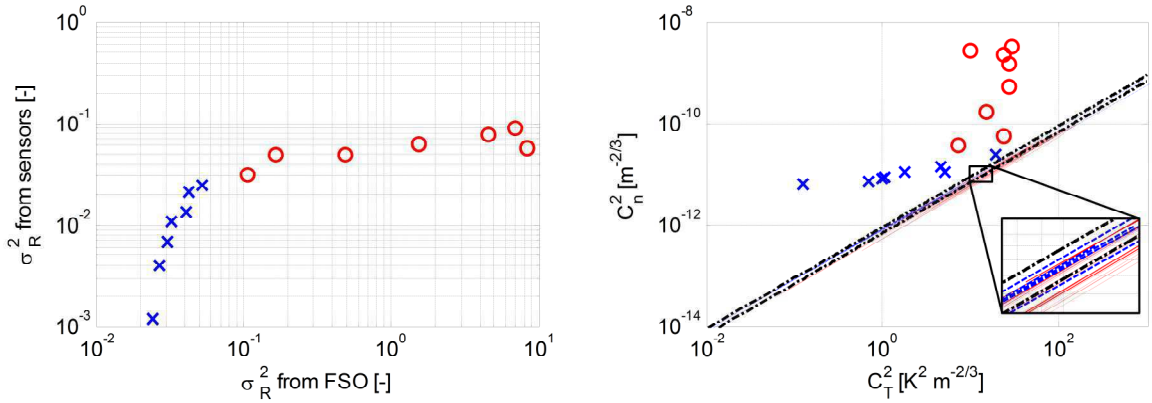

(a) (b)

Figure 22: Measured dependence of (a) Rytov variances in both channels derived from received optical signal and from thermal sensors measurements (symbols, red circles - channel 1, blue crosses - channel 2) and (b) C_n^2 theoretical relations (black dotted lines), C_n^2 derived from measured thermal distributions via Equations 21 and 12 (channel 1 red and channel 2 blue lines) and C_n^2 derived from measured of optical power on C_T^2 measured by the sensor line (symbols; red circles - channel 1, blue crosses – channel 2).

Partial Correlation in Turbulence at Channels

When considering deployment of wireless networks in urban areas the route diversity technique may be adopted in order to ensure higher link availability. To combat link failures FSO links can be arranged in several possible topologies thus offering diversity within the network to ensure link availability at all times.

The main aim during laboratory experiments was to analyze the route diversity for two links for case of intersecting the same turbulence area (i.e. channel 2 and part of channel 1) with the fraction of linearly increasing turbulence zone covering the major part of channel 1. This scenario corresponds to the real case when two links within the network are terminating at the same point, i.e. passing the common volume with the same or almost similar turbulence characteristic. Note one of the optical links is along the distant part influenced by the non-correlated turbulent flow. The measurement deployment can be seen in Figure 23.

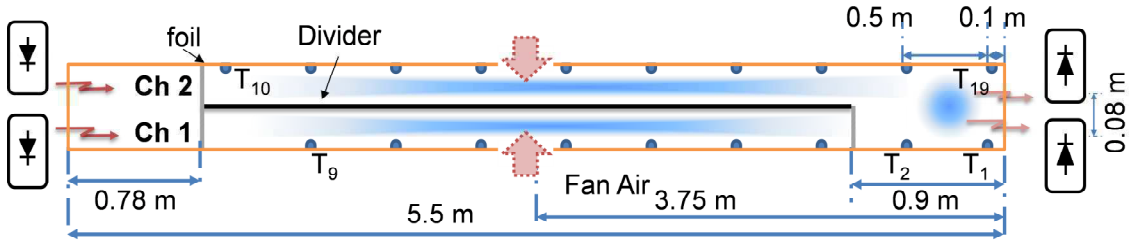

Figure 23: Deployment for measurement of partially correlated turbulences within channels.

Contrary to the previous case, the turbulence level in channel 2 was kept at Rytov variance value of 0.07. Compare the dependency of C_n^2 on C_T^2 (Figure 24), we observed that there is a decrease in the slope for the moderate turbulence condition, see inset in Figure 24.

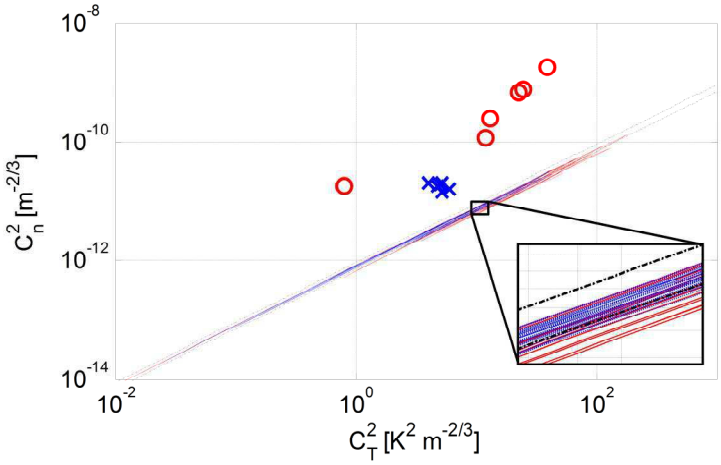

Figure 24: . Dependence of C_n^2 derived from measured of optical power measurements (red circles – channel1, blue crosses - channel 2) and from sensor line on thermal structural parameter in case of partially correlated turbulences, temperature measurements from channel 1 (red solid lines) and channel 2 (blue dashed lines) line sensors, compared with C_n^2 dependence derived from Equations 21 and 12 for the mean temperatures of 20 °C and 40 °C (black dotted lines).

In the next step, the diversity gains were derived in relation to Q-factors of received OOK signal from offline signal processing of both channels. The diversity gain against the Q-factor ratio between the channel with a low turbulence level and channels with high turbulence levels expressed by Q_{ch1}/Q_{ch2} is shown in Figure 25.

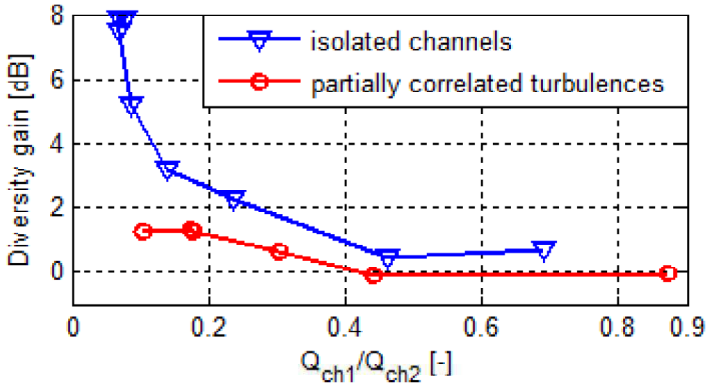

Figure 25: Comparison of diversity gains for two different turbulence scenarios with respect to Q-factor ratio between channels.

The SelC linear combiner samples the entire received signal through multiple branches and selects the branch with the highest SNR value or the irradiance level, provided the photodetectors receive the same amount of background radiation. The output is equal to the signal on only one of the branches and not the coherent sum of the individual photocurrents as is the case in MRC and EGC. This makes SelC suitable for differentially modulated, non-coherent demodulated subcarrier signals. In addition, SelC is of reduced complexity compared to the MRC and EGC and its conditional SNR is given by

$$\gamma_{SelC}(I) = \frac{R^2 A^2 I_{\max}^2}{2N\sigma^2}, \tag{22}$$

where $I_{max} = max\,(I_1, I_2, \ldots, I_N)$. The pdf of the received irradiance, $p(I_{\max})$, given by Equation 23, is obtained by first determining its cumulative density function (cdf) and then differentiating.

$$p(I_{\max}) = \frac{2^{1-N} N \exp\left(-y^2\right)}{I\sigma_i\sqrt{2\pi}}[1 + \operatorname{erf}(y)]^{N-1}, \tag{23}$$

where

$$y = \frac{\ln\left(I/I_0\right) + \sigma_l^2/2}{\sqrt{2}\sigma_l}. \tag{24}$$

From the measurements it was observed that the above mentioned analytical assumptions lead to overestimation of received signal deviation in case of two channels crossing non-correlated turbulences. As can be seen in Fig. 7 from comparison of probability density functions of the measured route diversity data and the statistically derived pdf by Equation 23 there is higher deviation in the measured selection diversity signal than expected.

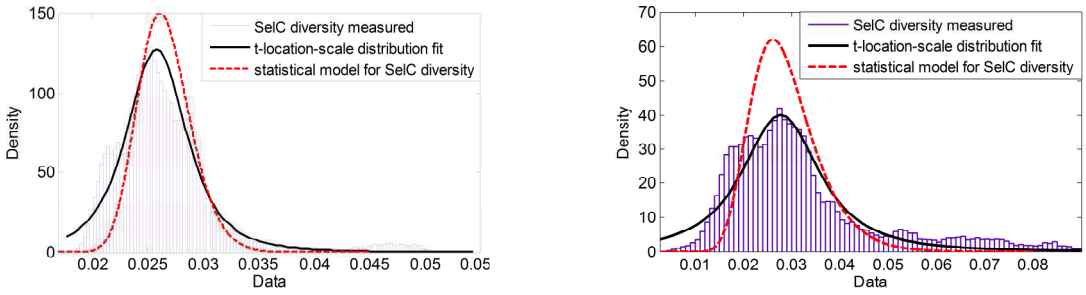

(a) $\sigma_1^2 = 0.0305,\ \sigma_2^2 = 1.5606$

(b) $\sigma_1^2 = 0.0608,\ \sigma_2^2 = 5.4235$

Figure 26: Examples from comparisons of measured and calculated Selection Combining diversity with Rytov variance in channels.

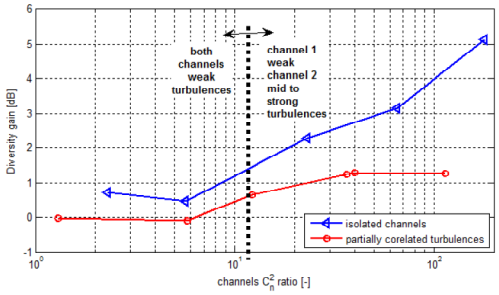

Figure 27: Comparison of diversity gains for two different turbulence scenarios with respect to C_n^2 ratio between channels.

CONCLUSION

This thesis deals with study of weather and turbulence influence on FSO links and utilization of combination of wavelength and route diversity. Statistical models from literature are related to measurement location or represent only theoretical assumptions. Czech Republic is situated in temperate climate and statistics was derived for urban environment. In order to investigate how an optical beam is affected by the atmosphere in real FSO links, measurement campaign was setup at the campus of the Czech Technical University in Prague. It contains three FSO links, a radio link and weather stations meteorological sensors.

First part of outdoor measurement is focused on investigation of building influence on FSO links. At first, FSO system statistics were derived based on developed network. Proper time span of calculation of refractive index structure parameter deviation from received optical power was determined by comparison with data obtained from temperature sensors. RMS errors of empirically derived log-normal and gamma-gamma model reaches minimal values. Relationship between temperature distribution along propagation path and the refractive index structure parameter was determined with correlation of up to 0.87.

The next part discusses the use of hybrid FSO-RF links. Statistics of received signal as well as availability of whole link were derived from long-term measurement. It was mentioned that complementary RF link is indispensable part of a high reliable link. Availability of FSO link without a RF link fluctuated from 97.74 to 99.999 % measured in monthly intervals. The overall availability can reach more than 99.71 %. In contrast, when using combination of FSO and RF link, availability of this hybrid FSO-RF link can be improved up to 99.999 %.

The last part of of outdoor tests investigates route diversity based on measurement of three FSO links. Parameters of log-normal PDF was derived from measured data of all links. It was proved, that sufficiently separated links are partially uncorrelated in term of refractive index structure parameter. Whis was taken in connection with coherent distance statistics for FSO networks. BER analysis of selection combining, depending on SNR was introduced for number of links in the range from 1 to 3. Comparison of BPSK and DPSK modulation technique is presented.

Diversity methodology was more in depth investigated based on indoor measurements performed in optical chamber at a laboratory, which was proposed and made within this work. Measurement of several modulation techniques including BPSK and 16QAM at different turbulence conditions was carried out. Only preliminary results are introduced in this thesis, because it has not been published yet. New model was derived for route diversity at different turbulence scenarios.

Experiment performed in the Newcastle, UK, is a part of European COST (Cooperation in Science and Technology) action withing group OPTICWISE (Optical Wireless Communications – An Emerging Technology). It investigates turbulence influence on two separated FSO channels. Advantage of this approach is possibility of creating turbulence with particular properties and generation of strong turbulence. As mentioned above, diversity gain reached up to 5 dB in case of totally separated channels, but in case of partially separated channels, maximum diversity gain was only about 1 dB. It limits utilization of route diversity techniques, when turbulence of both links is correlated.

The next research steps joint investigation with European teams of other effects resulting in impairment of propagation conditions typical for urban areas. New measurement campaigns were performed in summer months 2013 at CTU and other are planned in Newcastle to study influence of dust particles in the atmosphere.

References

[1] A. K. Mujamdar and J. C. Ricklin. *Free-Space Laser Communications: Principles and Advances.* New York: Springer, 2008.

[2] Propagation data required for the design of terrestrial free-space optical links. ed: Rec. ITU-R P.1817, 2007.

[3] L. Dordova and O. Wilfert. Free space optical link range determination on the basis of meteorological visibility. In *Proceedings of Radioelektronika 2009, 19th International Conference*, pages 333–336, 2009.

[4] M. S. Awan et al. Fso-relevant new measurement results under moderate continental fog conditions at graz and milan. In *Proceedings of Advanced Satellite Mobile Systems, 2008*, pages 116–121, 2008.

[5] L. C. Andrews and R. L. Phillips. *Laser beam propagation through random media.* Bellingham, Wash.: SPIE Press, 2nd edition, 2005.

[6] J. Libich and S. Zvanovec. An introduction to free-space optical communications. *Radioengineering*, 19:203–212, June 2010.

[7] O. Bouchet. *Free-space optics : propagation and communication.* London, Newport Beach, CA: ISTE, 2006.

[8] M. Grabner and V. Kvicera. Fog attenuation dependence on atmospheric visibility at two wavelengths for fso link planning. In *Proceedings of Loughborough Antennas & Propagation Conference*, pages 193–196, 2010.

[9] F. Nadeem and E. Leitgeb. Dense maritime fog attenuation prediction from measured visibility data. *Radioengineering*, 19:223–227, June 2010.

[10] N. Araki and H. Yashima. A channel model of optical wireless communications during rainfall. In *2nd International Symposium on Wireless Communications Systems 2005 (ISWCS 2005)*, pages 205–209, 2005.

[11] C. P. Colvero et al. Fso systems: Rain, drizzle, fog and haze attenuation at different optical windows propagation. In *Microwave and Optoelectronics Conference 2007 (IMOC 2007)*, pages 563–567, 2007.

[12] M. Grabner and V. Kvicera. On the relation between atmospheric visibility and optical wave attenuation. In 16^{th} *Mobile and Wireless Communications Summit, 2007*, pages 1–5, 2007.

[13] Prediction methods required for the design of terrestrial free-space optical links. ed: Rec. ITU-R P.1814.

[14] S. Kaneko and T. Hamai. Evaluation of a free-space optical mesh network communication system in the tokyo metropolitan area. *Journal of oprical networking*, 1:414–423, November 2002.

[15] L. C. Andrews. *Field guide to atmospheric optics.* Bellingham, Wash.: SPIE, 2004.

[16] L. C. Andrews, R. L. Phillips, and C. Y. Hopen. *Laser beam scintillation with applications.* Bellingham, Wash.: SPIE Press, 2001.

[17] Z. Ghassemlooy et al. Free-space optical communication using cubcarrier modulation in gamma-gamma atmospheric turbulence. In *Proceedings of the* 9^{th} *internacional conference on transparent optical networks*, volume 3, pages 156–160, 2007.

[18] W. Xueying et al. A study on atmospheric turbulence effects in full-optical free-space communication systems. In *6th International Conference on Wireless Communications Networking and Mobile Computing (WiCOM)*, pages 1–5, 2010.

[19] et al. H. Moradi. Ber analysis of optical wireless signals through lognormal fading channels with perfect csi. In *IEEE 17th International Conference on Telecommunications (ICT)*, pages 493–497, 2010.

[20] A. Jurado-Navas et al. Efficient lognormal channel model for turbulent fso communications. In *Electronics Letters*, volume 43, pages 178–180, 2007.

[21] M. Uysal et al. Error rate performance analysis of coded free-space optical links over gamma-gamma atmospheric turbulence channels. In *IEEE Transactions on Wireless Communications*, volume 5, pages 1229–1233, 2006.

[22] H. Moradi, M. Falahpour, H.H. Refai, P.G. LoPresti, and M. Atiquzzaman. Reconfiguration modeling of reconfigurable hybrid fso/rf links. In *Communications (ICC), 2010 IEEE International Conference on*, pages 1–5, 2010.

[23] H. Moradi, M. Falahpour, H.H. Reafi, P.G. LoPresti, and M. Atiquzzaman. Availability modeling of fso/rf mesh networks through turbulence-induced fading channels. In *INFOCOM IEEE Conference on Computer Communications Workshops , 2010*, pages 1–5, 2010.

[24] H. Henniger et al. Maritime mobile optical-propagation channel measurements. In *IEEE Int. Conf. on Communications*, pages 1–5, 2010.

[25] A. Kolmogorov. The local structure of turbulence in incompressible viscous ?uid for very large reynolds numbers. *Doklady Akad. Nauk, S.S.S.R.*, pages 301–305, 1941.

Publikace vztahující se k tématu disertační práce

Publikace v impaktovaných časopisech:

Libich J. (50%), Zvanovec. S. Influences of turbulences in near vicinity of buildings on free-space optical links, IET MICROWAVES ANTENNAS & PROPAGATION. pp 1039-1044 Jun 2011.
Citováno: bez citace

Zvanovec J., Perez J., Ghassemlooy Z., Rajbhandari S., Libich J. (20%) . Route diversity analyses for free-space optical wireless links within turbulent scenarios, OPTICS EXPRESS, pp 7641-7650, Mar 2013.
Citováno: bez citace

Publikace v recenzovaných časopisech

Patenty

Dvorak P., Libich J. (50%). Diferenciální teplotní senzor. [Funkční vzorek]. 2010.
Libich J. (50%), Zvanovec S.. Senzorová sada umožňující kontinuální měření turbulentních zón v blízkosti budov za účelem nalezení jejich vlivu na bezdrátové optické systémy. [Funkční vzorek]. 2010.

Publikace excerpované WOS

Libich J. (33%), Zvanovec S., Mudroch M. Mitigation of time-spatial influence in free-space optical networks utilizing route diversity, Proceedings of SPIE. 24-26 Jan 2012.

Dvorak P., Libich J. (33 %), Zvanovec S.. Combined Measured Characteristics of Microwave Radiometer and Free-Space Optical Link, IEEE AP-S/URSI Conference - Paper #2121. 26-30 Mar 2012.

Publikace ostatní:

Libich, J. (50%); Zvanovec, S.; "Measurement statistics of three joint wireless optical links," International Workshop on Optical Wireless Communications (IWOW), vol., no., pp.1-3, 22-22 Oct. 2012.

Libich, J. (33%), Zvanovec, S., Mudroch, M., "Mitigation of time-spatial influence in free-space optical networks utilizing route diversity", SPIE Photonics West 2012 - Free-Space Laser Communication Technologies XXIV, March 2012.

Libich, J. (33%); Mudroch, M.; Zvanovec, S.; , "Atmosphere analysis and measurements via free-space optical network," 22nd International Conference on Electrical Communications and Computers (CONIELECOMP), vol., no., pp.230-233, 27-29 Feb. 2012

Libich, J. (25%); Mudroch, M.; Dvorak, P.; Zvanovec, S.; , "Performance analysis of hybrid FSO/RF link," 6th European Conference on Antennas and Propagation (EUCAP), vol., no., pp.1235-1238, 26-30 March 2012

Libich J. (50%) and Zvanovec S., “Utilization of Route Diversity in Free-Space Optical Networks,” Avionics, Fiber-Optics and Photonics Technology Conference (AVFOP), 2011

Zvanovec and Libich J. (50%), "Analysis of rain influence on joint millimeter and optical elevated links," in Proceedings of the 5th European Conference on Antennas and Propagation (EUCAP), 2011, pp. 174-177

Publikace ostatní

Publikace v impaktovaných časopisech:

Libich J. (25%), Dvorak P. (25 %), Petr Piksa, Stanislav ZVANOVEC, „Correction of Thermal Deviations in Fabry-Perot Resonator Based Measurements of Specific Gases in Millimeter Wave Bands“, Radioengineering, submitted 17th November 2011 and accepted.

Publikace v recenzovaných časopisech

Patenty

Publikace excerpované WOS

Publikace ostatní

Procentuální podíl všech spoluautorů u uvedených publikací je rovnoměrný.

SUMMARY

Requirements for the network throughput have been growing very quickly. Importance of free space optics as last-mile connection has increased in recent years. Contrary to classic radio band communication systems, FSO offer higher bandwidth and consequently higher data rates up to 10 Gbps. Higher safety is reached by invisible narrow optical beam, whose divergence is typically around units of milliradians. Another advantage is no need of licensing and no interference with radio waves. Fast deployment owing to no need of street digging makes this technology cheaper in contrast to fiber optics. Unfortunately, optical beam is strongly influenced by atmospheric condition and by weather effects. Distance of the link given by its power budged is limited by many factors. Ubiquitous turbulence causes scintillation - fluctuation of the received optical power resulting from spreading and wandering of the optical beam. Dominant effect resulting in attenuation of an optical wave caused by weather is fog. Aim of this thesis is to find a statistic model of based on long-term measurement of received optical power and laboratory experiments focused on investigation of utilization of route diversity for turbulence faded channels. Statistical models of propagation medium parameters in combination with route diversity in FSO networks have been found based on outdoor and laboratory measurement.

RESUMÉ

Bezdrátové optické spoje (FSO) představují perspektivní komunikační technologii, využívající optického svazku pro přenos informace volným prostředím. Mezi jejich hlavní výhody patří zejména vysoká přenosová rychlost, vysoká bezpečnost přenosu díky úzkému svazku, provoz v bezlicenčním pásmu a rychlá instalace. Přenos je bohužel silně ovlivněn atmosférickými jevy a počasím. Tato disertační práce se zaměřuje na využití diversitních technik v FSO sítích. Zaměřuje se na využití hybridních FSO spojů v kombinaci s trasovou diversitou. Statistické modely jsou odvozeny z dlouhodobých měření v reálném prostředí a z měření v laboratorních podmínkách.